analytical chemistry

Article

Cite This: Anal. Chem. 2019, 91, 5777−5785

pubs.acs.org/ac

Ultrasensitive Sensor Using Quantum Dots-Doped Polystyrene Nanospheres for Clinical Diagnostics of Low-Volume Serum Samples

Zhenhua Chen,[†] Peng Li,[†] Zhigao Zhang,[†] Xiangming Zhai,[†] Junyu Liang,[†] Qiong Chen,[†] Kun Li,[†] Guanfeng Lin,[†] Tiancai Liu,[*,†,‡,§] and Yingsong Wu[*,†,§]

[†]Institute of Antibody Engineering, School of Laboratory Medicine and Biotechnology, and [‡]Guangdong Provincial Key Laboratory of Construction and Detection in Tissue Engineering, Southern Medical University, Guangzhou 510515, Guangdong, People's Republic of China

Supporting Information

ABSTRACT: Development of sensitive homogeneous assays is a high-priority research target for clinical diagnostics. Quantum dots (QDs) present favorable photophysical properties, which implies their potential as an exceptional dye in fluorescence detection. QDs-based biosensors have been described in the literature; however, few of them have truly progressed to widespread clinical usage. In this work, a chemiluminescent homogeneous detecting biosensor is fabricated using QDs-doped polystyrene nanospheres to sensitively detect biomarkers in low-volume serum samples. Phthalocyanine-dyed and QDs-encapsulated carboxylate-functionalized polystyrene nanospheres with surface carboxyl groups (PPs and QPs, respectively) were fabricated and served as triggers and fluorescent probes, respectively, in this biosensing system. In this sandwich-format immunoassay, the PPs produced singlet oxygen once sensitized by 680 nm diode lasers, and the QPs, conjugated with antibodies, and then reacted with the singlet oxygen in the presence of specific antigens and emitted anti-Stokes fluorescence with wavelengths around 605 nm, as a result of fluorescence resonance energy transfer (FRET) within the QPs. We demonstrated the determination of carcinoembryonic antigen as a model protein target in 25 μL of serum samples with an unprecedented detection limit of 2.56×10^{-13} M (46 pg/mL) using this biosensor. Furthermore, excellent correlations ($R^2 = 0.99718$, $n = 107$) were obtained between utilizing this biosensor and commercialized chemiluminescence immunoassay kits in clinical serum detection. These results demonstrate that our flexible and reliable biosensor is suitable for direct integration into clinical diagnostics, and it is expected to be a promising diagnostic tool for early detection and screening tests as well as prognosis evaluation for patients.

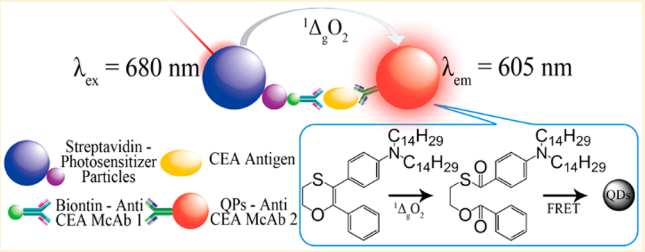

Quantum dots (QDs) are very small semiconductor particles in the 2−10 nm size range and have been a subject of interest since their discovery in the 1980s.[1,2] QDs possess numerous unique optoelectronic properties, including size- and composition-dependent emission,[3] broad excitation range, high quantum yield, symmetrical and narrow emission peaks, and superior photostability. Therefore, QDs have been implemented in transistors, indoor lighting, diode lasers, energy generation, and biological imaging.[4−9] However, suffering from the colloidal nature of QD dispersions, their application in biosensing has been less successful owing to the physical or chemical stability issues and insufficient sensitivity in biological matrixes. Biosensing applications require agents that are water soluble and capable of biological conjugation, which QDs—being created by colloidal synthetic procedures—tend not to be, although several approaches would help to improve their stability in aqueous solution.[10−12] Nevertheless, QDs cannot be easily functionalized with amino acids using the common coupling agent 1-ethyl-3-(3-dimethylaminopropyl) carbodiimide hydrochloride (EDC). It has been reported that exposure to excess EDC could bring about irreversible precipitation and quenching of QDs.[13]

Cancer is a major public health problem worldwide. A total of 1,735,350 new cancer cases and 609,640 cancer deaths are projected to occur in the United States in 2018.[14] Therefore, there is an urgent need for a sensitive and accurate method for detecting tumor markers in serum, body fluids, or tissues. With the development of clinical diagnostics, numerous methods have been established for the detection of biomarkers in serum samples. These include enzyme-linked immunosorbent assay,[15,16] radioimmunoassay,[17−19] and time-resolved fluoroimmunoassay.[20−22] However, measurement of ligand−receptor binding by the above methods requires the physical separation of the bound and free labeled ligand or receptor. Time-consuming and laborious washing processes are necessary to avoid nonspecific absorption and strongly fluorescent backgrounds, and these procedures can result in

Received: January 1, 2019
Accepted: April 3, 2019
Published: April 3, 2019

DOI: 10.1021/acs.analchem.9b00010
Anal. Chem. 2019, 91, 5777−5785

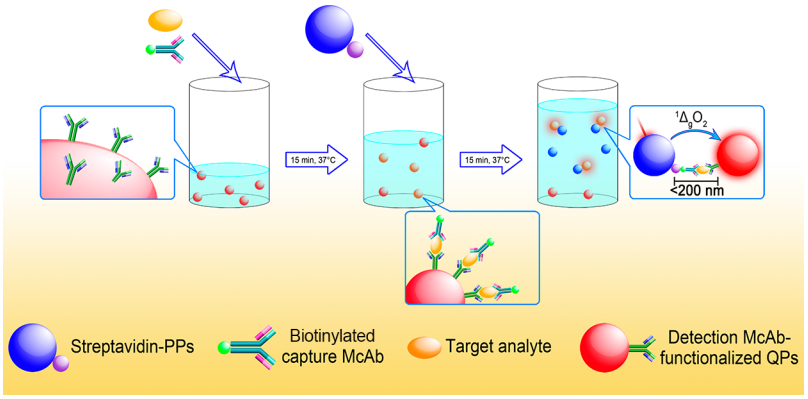

Figure 1. Schematic representation of the homogeneous quantitative assay using CEA as a model analyte. In the presence of CEA, PPs and QPs are bound together. The singlet oxygen ($^1\Delta_gO_2$) molecules are formed by irradiation of the PPs at a 680 nm laser and diffuse only a short distance before being captured by the QPs, triggering a chemical cascade leading to emission from the QDs, which can be measured at 605 nm.

changes of the structure or conformation of the biomolecules and weaken the specificity and sensitivity of the immunoassay. In contrast to heterogeneous methods, homogeneous assays, such as chemiluminescence immunoassay (CLIA)[23,24] and chemiluminescent enzyme immunoassay,[25,26] avoid this troublesome step and are therefore theoretically capable of better performance. Nevertheless, these assays also face several limitations. They are susceptible to matrix effects, and their sensitivity is often inadequate.

QDs-based fluorescence resonance energy transfer (FRET) has proven itself to be a promising tool for biomolecule sensing owing to the unique advantages over the common organic dye-based FRET sensing system.[27,28] Actually, there exist two main obstacles in achieving successful practical application. First of all, the best QD materials are synthesized in hydrophobic surfactants that prevent direct aqueous solubilization, even though several methods have been developed to impart their water solubility. Traditional methods of water solubilization and functionalization of QDs either have low quantum yield or cause irreversible precipitation of the sample.[29,30] Thus, common QDs-based FRET detecting systems have been hindered by the insufficient labeling chemistries and the unrobustness in polar solvents, particularly in clinical media such as serum or plasma. Second, high-efficiency FRET relies on the proper donor−acceptor distances, which should be in the range of approximately 1−10 nm. For detecting macromolecules (antigens or antibodies), the donor−acceptor distance would be too large to establish an efficient FRET process because of the large size of the immunocomplex.

Herein, we present a novel QDs-doped nanospheres-based, chemiluminescent homogeneous sensor for sensitive and specific detection of biomolecules in small-volume serum samples. As illustrated in Figure 1, this biosensor consists of two kinds of polystyrene nanoparticles, photosensitizer particles (PPs) and QD-doped particles (QPs), respectively. In the presence of target analyte, the PPs−QPs distance would be shortened by specific binding. When a suspension of PPs is irradiated by a 680 nm laser, the singlet oxygen is formed within each particle and rapidly diffuses only a short distance. Thus, only the bound QPs, which are within the binding distance of a PP, are likely to react with singlet oxygen and undergo subsequent FRET process. The reaction with singlet oxygen and the subsequent FRET emission is strongly dependent on the formation of coupled nanospheres pairs, which is proportional to the concentration of target analyte in the detecting solution. The principle of the method is similar to AlphaLISA immunoassay. When compared with AlphaLISA, the present biosensor provides the higher FRET efficiency and greater flexibility due to the broad excitation profiles and high extinction coefficient of QDs. Furthermore, the excellent optical properties of QDs render this novel biosensor as a robust reporter for developing highly sensitive detection capable of simultaneous quantification of multianalytes. A quantitative model assay for carcinoembryonic antigen (CEA) was constructed using streptavidin-conjugated PPs (SAv−PPs) and biotinylated anti-CEA monoclonal antibody (McAb). To demonstrate the reliability of the proposed sensor, several assay parameters, including repeatability, intermediate precision, recovery, linearity, assay range, and feasibility, were further measured.

EXPERIMENTAL SECTION

Reagents and Instrumentation. Antihuman CEA monoclonal antibodies (McAbs) (clones 5909 SP-5 and 5910 SPTN-5) were purchased from Medix Biochemica. CEA antigen was obtained from Fitzgerald Industries International. OptiLink carboxylate-modified microparticles (CM-Ps) were purchased from Thermo Fisher Scientific. Silicon 2,9,16,23-tetra-*tert*-butyl-29*H*,31*H*-phthalocyanine trihexyl(methoxy)silane (SiPc, 95%) and 4-(2-phenyl-5,6-dihydro-1,4-oxathiin-3-yl)-*N*,*N*-ditetradecylbenzenamine (DTB, 95%) were purchased from WuXi AppTec, China. All other chemicals were arrived as analytical grade and without further purification before being used. Additionally, serum samples were granted by Nanfang Hospital, China.

Preparation of QPs and PPs. Hydrophobic trioctylphosphine oxide-annealed core/shell CdSe/ZnS QDs were assembled by the procedures reported in our earlier studies and the literature.[31,32] The QDs concentration was determined by absorbance measurements assuming molar absorptivities of 3.4×10^6 M^{-1} cm^{-1} at 595 nm. The QPs were prepared by modification of a published method.[33] Fifty microliters of CM-Ps were washed three times and resuspended in 0.8 mL of butanol by thorough sonication. One hundred microliters of as-prepared QDs (36.2 mM in hexane) and 100 μL of DTB (30.3 mM in hexane) were mixed and added dropwise into the vigorously stirred CM-Ps suspension. The mixtures were stirred for 30 min at room temperature and sonicated three times (1 min per time) at 10 min intervals until the QDs had penetrated sufficiently into the particles. The prepared QPs

DOI: 10.1021/acs.analchem.9b00010
Anal. Chem. 2019, 91, 5777−5785

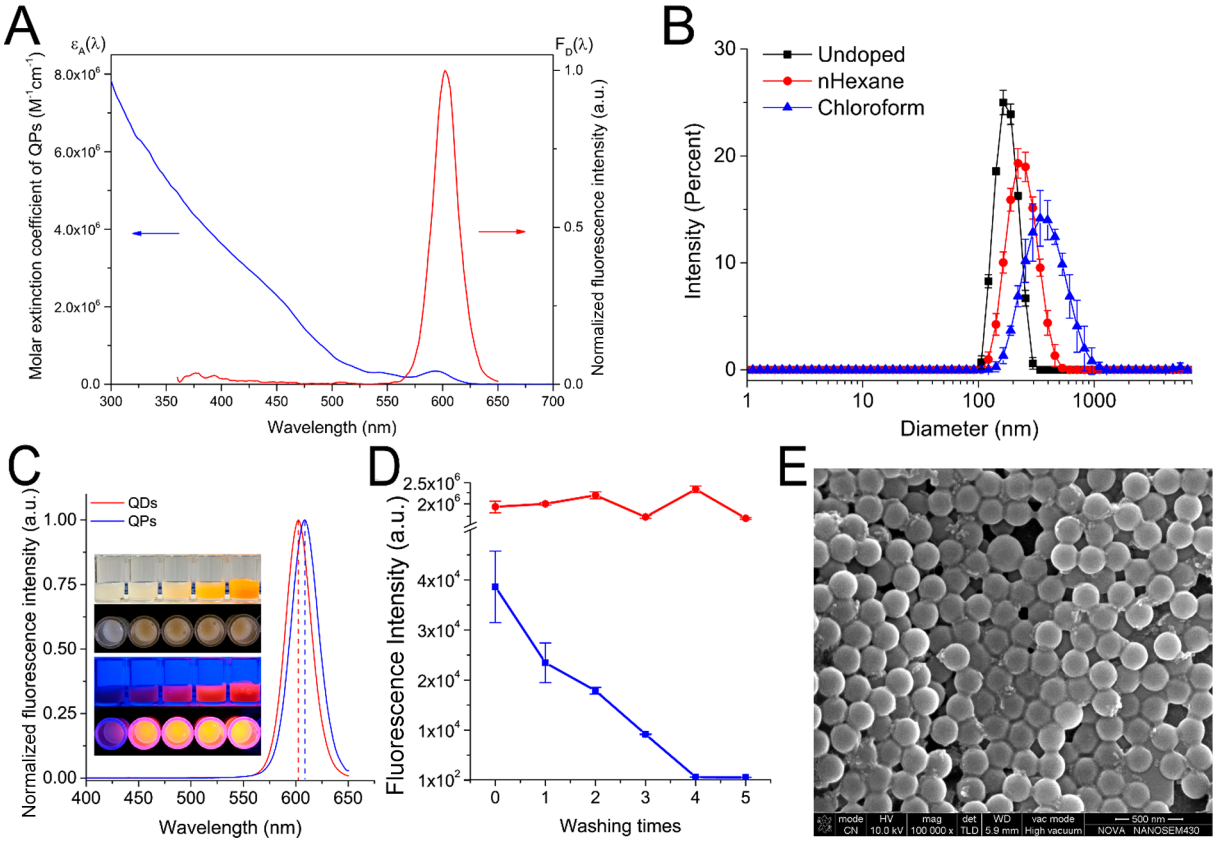

Figure 2. Preparation and characterization of QDs and QPs. (A) Molar absorptivity (blue curve) and normalized fluorescence spectra (red curve) of as-prepared QDs (3 μM in hexane). (B) Size distributions by intensity of undoped CM-Ps (black squares) and QPs (red circles for QPs obtained from hexane and blue triangles for those obtained from chloroform, respectively). (C) Fluorescence spectra of QDs (red curve) and QPs (blue curve). The inset shows photographs of QPs at different concentrations under natural light and UV light. (D) Fluorescence intensity of washing supernatant (blue curve) and QPs (red curve). (E) Field emission scanning electron microscopy (FESEM) image of QPs.

were purified by washing four times with 50% ethanol, and then were suspended in 10% ethyl alcohol solution. The QPs were packaged at a concentration of 5 mg/mL after dilution with 10% ethyl alcohol solution and stored at 4 °C.

PPs were prepared by heating and swelling. All of the procedures for preparing the PPs were conducted in the absence of light. Details of the preparation are as follows. Fifty milligrams of SiPc (36.7 μmol) and 50 mg of CM-Ps were suspended in 5 mL of swelling solution (ethylene glycol/benzyl alcohol/water 8:1:1, v/v). The mixture was stirred for 10 min at 120 °C under argon before being cooled to room temperature. To remove the free SiPc, washing processes were performed. The PPs were diluted and packaged at a final concentration of 5 mg/mL with 10% ethanol and stored at 4 °C in the dark.

Functionalizing QPs and PPs. QPs and PPs were functionalized by conjugation of antibodies (clone 5909 SP-5) and streptavidin, respectively, via covalent attachment. Proteins were purified on molecular weight cutoff (MWCO) spin columns (50 kDa for antibodies and 30 kDa for streptavidin, both from Millipore) before conjugation and diluted to a concentration of 1 mg/mL in coupling buffer (25 mM phosphate buffer, pH 7.0). To avoid bridging of the particles and cross-linking of the protein to itself, a two-step procedure was chosen. Briefly, 1 mg of microparticles was suspended in 0.4 mL of activating buffer (25 mM MES buffer, pH 6.1). Then, 10 μL of EDC (10 mg/mL in 25 mM MES buffer, pH 6.1) was mixed with 90 μL of sulfo-*N*-hydroxysulfosuccinimide (sulfo-NHS, 10 mg/mL in 25 mM MES buffer, pH 6.1), and the mixed solution was added into the suspension of microparticles. After 30 min of incubation at room temperature, the semistable NHS-ester was produced by reaction of the carboxyl groups on the surface of the particles. Unreacted sulfo-NHS and EDC were separated by washing three times with washing buffer (150 mM NaCl, 0.05% Tween-20, and 0.05% Proclin-300 in 25 mM Tris−HCl, pH 7.8). The particles pellet was resuspended in 0.4 mL of coupling buffer by sonication, 60 μL of protein solution was added into the suspension of microparticles, and the volume of the mixture was finally made up to 0.5 mL with coupling buffer. The mixture was incubated for 2 h at room temperature with gentle mixing. Ethanolamine (1.3 μL) was pipetted into the reaction mixture, and a further 30 min of incubation was cast. A three-times washing process was accessed to remove unbound components or proteins prior to adding blocking buffer (20 mg/mL BSA in 25 mM phosphate buffer, pH 7.4). The functionalized QPs and PPs were suspended in blocking buffer by sonication and were, respectively, incubated for another 30 min with gentle shaking to cap unbound hydrophobic sites that remained on the outside of the microparticles and to prevent clumping. Finally, the functional QPs and PPs were purified by a three-times washing process using washing buffer and resuspended in storing buffer (10 mg/mL BSA, 50 mg/mL trehalose, 200 mg/mL sucrose, and 0.05% Proclin-300 in 25 mM Tris−HCl, pH 8.0) and stored at 4 °C. It is important for functionalized PPs to be kept away from light.

DOI: 10.1021/acs.analchem.9b00010
Anal. Chem. 2019, 91, 5777−5785

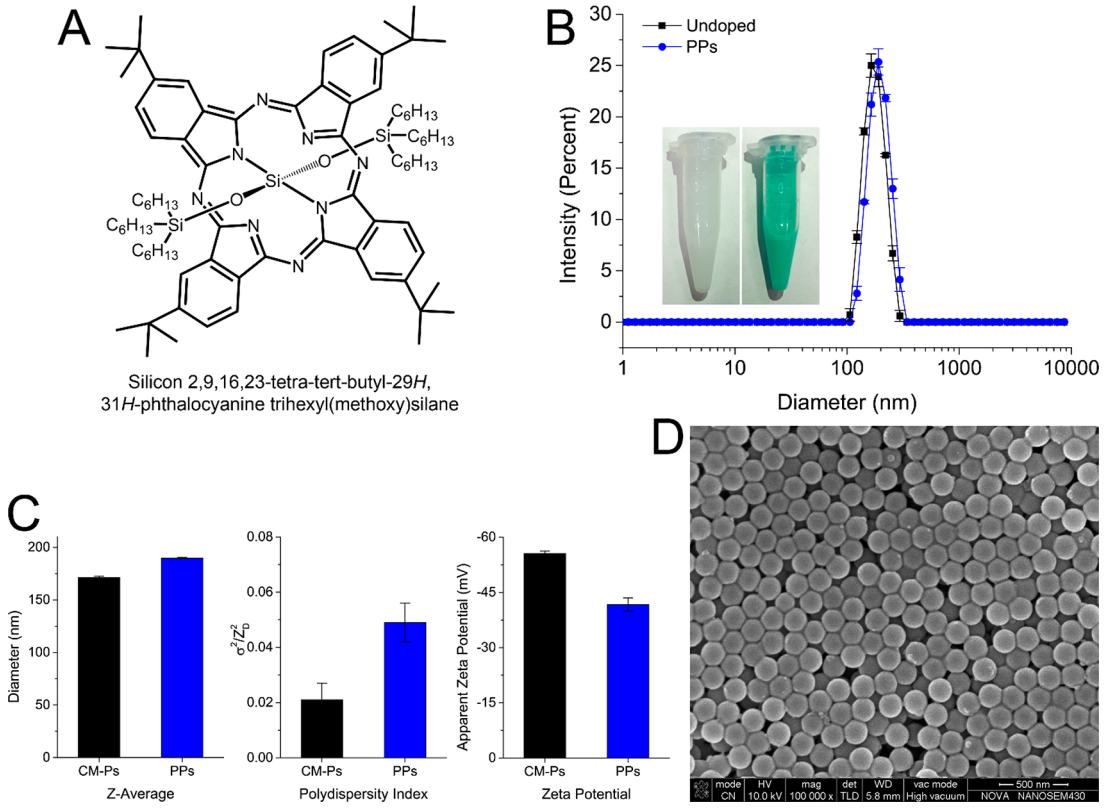

Figure 3. Preparation and characterization of PPs. (A) Photosensitizer: silicon phthalocyanine. (B) Size distributions by intensity of undoped CM-Ps (black squares) and PPs (blue circles). The inset shows photographs of undoped CM-Ps (left) and PPs (right) under natural light. (C) *Z*-average size, polydispersity index, and ζ-potential of undoped CM-Ps and PPs. (D) FESEM image of PPs.

Characterization of QPs and PPs. Absorption spectra (UV2550 UV−vis spectrophotometer, Shimadzu) and photoluminescence (PL) spectra (LS-55 fluorescence spectrometer, PerkinElmer) were recorded in hexane for the QDs and DTB samples, respectively. Field emission scanning electron microscopy (FESEM) was carried out using a NOVA NanoSEM430 microscope (FEI) operating at an acceleration voltage of 10 kV. Dynamic light scattering (DLS) analysis was carried out in a Zetasizer Nano S90 size analyzer (Malvern). Flow cytometry analysis was carried out in a LSRFortessa X-20 cell analyzer (BD Life Sciences) to evaluate the activity of protein molecules after conjugation.

Biotinylation of Antibodies and Homogeneous Immunoassay. Prior to biotinylation, 1 mg of antibodies (clone 5910 SPTN-5) was diluted in 0.5 mL of carbonate buffer (0.1 M, Na_2CO_3/$NaHCO_3$, pH 9.5) and was purified on a 50 kDa MWCO spin column. The purified antibodies were mixed with 16 μL of biotin *N*-hydroxysuccinimide ester solution (10 mM, dimethyl sulfoxide) and incubated at room temperature for 4 h. The biotinylated antibodies were purified and concentrated on a 50 kDa MWCO spin column with storing buffer.

The functionalized QPs and biotinylated antibodies were diluted with assay buffer (150 mM NaCl, 10 mg/mL BSA, and 0.3% TritonX-100 in 10 mM $Na_2HPO_4{\cdot}12H_2O$, pH 7.4), and the detecting solution was made up by mixing the assay buffer with aliquots containing 10 μg/mL QPs and 2.5 μg/mL biotinylated antibodies. To each immunoassay well, 50 μL of as-prepared detecting solution and 25 μL of the standard or serum sample were added. The mixtures were incubated with shaking at 37 °C for 15 min. Diluted PPs solution (175 μL, 0.1 mg/mL, 10 mM phosphate buffer, pH 7.0) was added, and 15 min incubation with shaking at 37 °C in the absence of light was performed. The fluorescence signal was measured on an EnSpire multimode plate reader (PerkinElmer).

RESULTS AND DISCUSSION

Validation of Hydrophobic QDs and QPs. QDs of high quality are normally manufactured in hydrophobic solvents to preclude direct aqueous solubilization. The PL spectra of the as-prepared QDs were measured and are shown in Figure 2A. The fluorescence emission was maximized at about 605 nm with a full width at half-maximum (fwhm) of about 25 nm, and the shape of the emission peak was symmetric and narrow. Furthermore, the excellent photoproperties of the as-prepared QDs were evident from the negligible overlap between the absorption and emission spectra.

In order to enhance the dispensability and photochemical stability of colloidal QDs, encapsulating QDs into water-dispersed spheres is preferred. Up to now, two major strategies were developed for encapsulation. In the first, hydrophobic QDs are passively absorbed and trapped into shaped polystyrene latex nanoparticles via chemical or physical processes, such as swelling in suitable solvent. In the second one, QDs are integrated into polystyrene particles during the polymerization.[34] The former strategy was chosen in this study for its simplicity and high efficiency. This process offers several advantages. First, embedding in polystyrene nanospheres provides a hydrophobic environment, which is indispensable for maintaining the brightness and stability of QDs. Moreover, the use of nanometer-sized spheres increases the contact surface upon which antibodies and antigens can react.

DOI: 10.1021/acs.analchem.9b00010
Anal. Chem. 2019, 91, 5777−5785

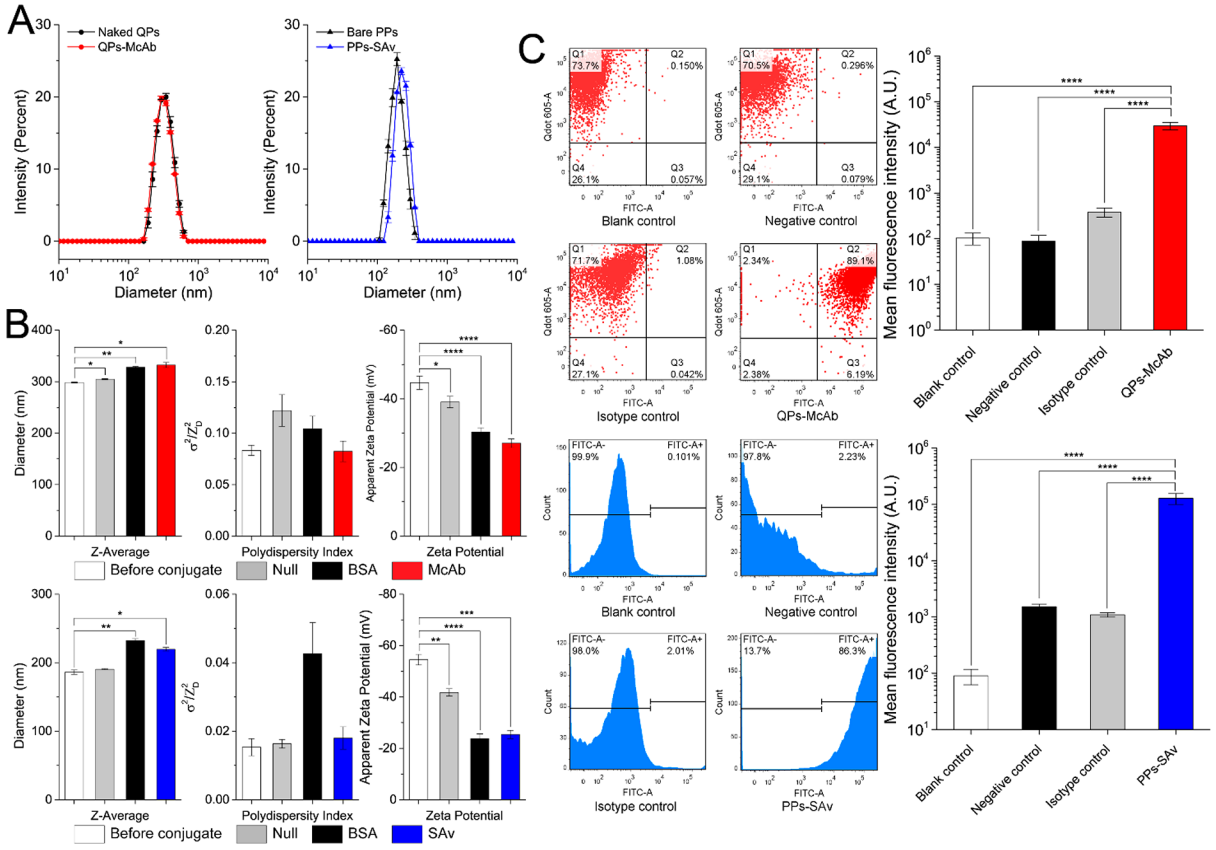

Figure 4. DLS and flow cytometry analysis of functional nanoparticles. (A) Size distributions by intensity of naked QPs (black circles), QPs which were functionalized with antibodies (red circles), bare PPs (black triangles), and streptavidin-coupling PPs (blue triangles). (B) *Z*-average size, polydispersity index, and ζ-potential of QPs (top panel) and PPs (bottom panel). (C) Populations and MFI of functional QPs (top panel) and PPs (bottom panel). Notably, naked QPs/PPs and BSA-conjugated QPs/PPs served as the blank control and negative control, respectively, in flow cytometry analysis. (One-way analysis of variance was used in comparing *Z*-average size, ζ-potential, and MFI of different samples: *, $P < 0.05$; **, $P < 0.01$; ***, $P < 0.001$; ****, $P < 0.0001$; 95% of confidence interval.)

Furthermore, the carboxyl groups on the surfaces of nanospheres are reactive toward the amine groups of biomolecules after activation with carbodiimide reagents. Proteins such as antibodies can be easily and selectively attached while retaining their immunoreactivity. Typically, incorporation of QDs with polystyrene latex nanoparticles could be achieved by swelling the beads in a solvent mixture containing chloroform.[35,36] However, as shown in Figure 2B and Figure S1, instead of encapsulating QPs via chloroform, we have found that the QPs which were fabricated in hexane−butanol solution presented the better dispersibility and narrower size distribution range in DLS analysis in this study. The characterization of QPs was employed to explore various parameters to achieve optimal conditions such as encapsulating time, concentration of hexane, and the usage of QDs. As shown in Figure S2, 30 min of encapsulation, 20% of hexane, and 0.6 mg/mg (QDs: CM-Ps) of QDs usage was determined to achieve optimal size and fluorescence intensity of QPs. In order to confirm the influence of the swelling process on optical properties of the as-prepared QDs, the PL spectra of the QDs in hexane and QPs suspended in PBS buffer were measured, respectively. As shown in Figure 2C, no significant spectral shift was found, suggesting that fabrication of the QPs cause no significant impact to the optical properties of the as-prepared QDs. Additionally, to evaluate the stability of the QDs within the QPs, the QPs were centrifuged and washed several times with 50% ethanol (v/v). The washing supernatants were collected and were analyzed by a Wallac 1420 multilabel counter (PerkinElmer). As shown in Figure 2D, the fluorescence intensity of the washing supernatants was found to decrease as the number of washes increased. In contrast, the fluorescence intensity of the QPs remained at a high level. This result indicated that the QDs had been trapped tightly in the polystyrene latex nanoparticles and did not escape from latex particles. As shown in Figure 2E, the QPs exhibited a narrow grain size distribution with an average diameter of 209.5 ± 1.4 nm based on characterization by FESEM.

Evaluation of Photosensitizer Particles. The biosensor reported here is designed to be stimulated by 680 nm solid-state laser light sources. This procedure permits the QDs' photoluminescence to be selectively discriminated from the autofluorescence of serum components, resulting in minimal background signal, higher sensitivity, and higher accuracy compared with conventional biosensing methods. For this purpose, a photosensitizer, SiPc (Figure 3A), was selected, which can activate $^1\Delta_gO_2$ to serve as single transmitters. The desired quantity of SiPc was embedded in CM-Ps, offering a stable environment to protect the SiPc during the activation of $^1\Delta_gO_2$, as well as greatly amplifying the signal. In this way, PPs with an average diameter of 166.8 ± 9.9 nm were synthesized. DLS data and the FESEM image of the PPs are shown in Figure 3B−D.

Functionalizing Nanoparticles. The nanospheres were functionalized by conjugation of biomolecules via covalent

DOI: 10.1021/acs.analchem.9b00010
Anal. Chem. 2019, 91, 5777−5785

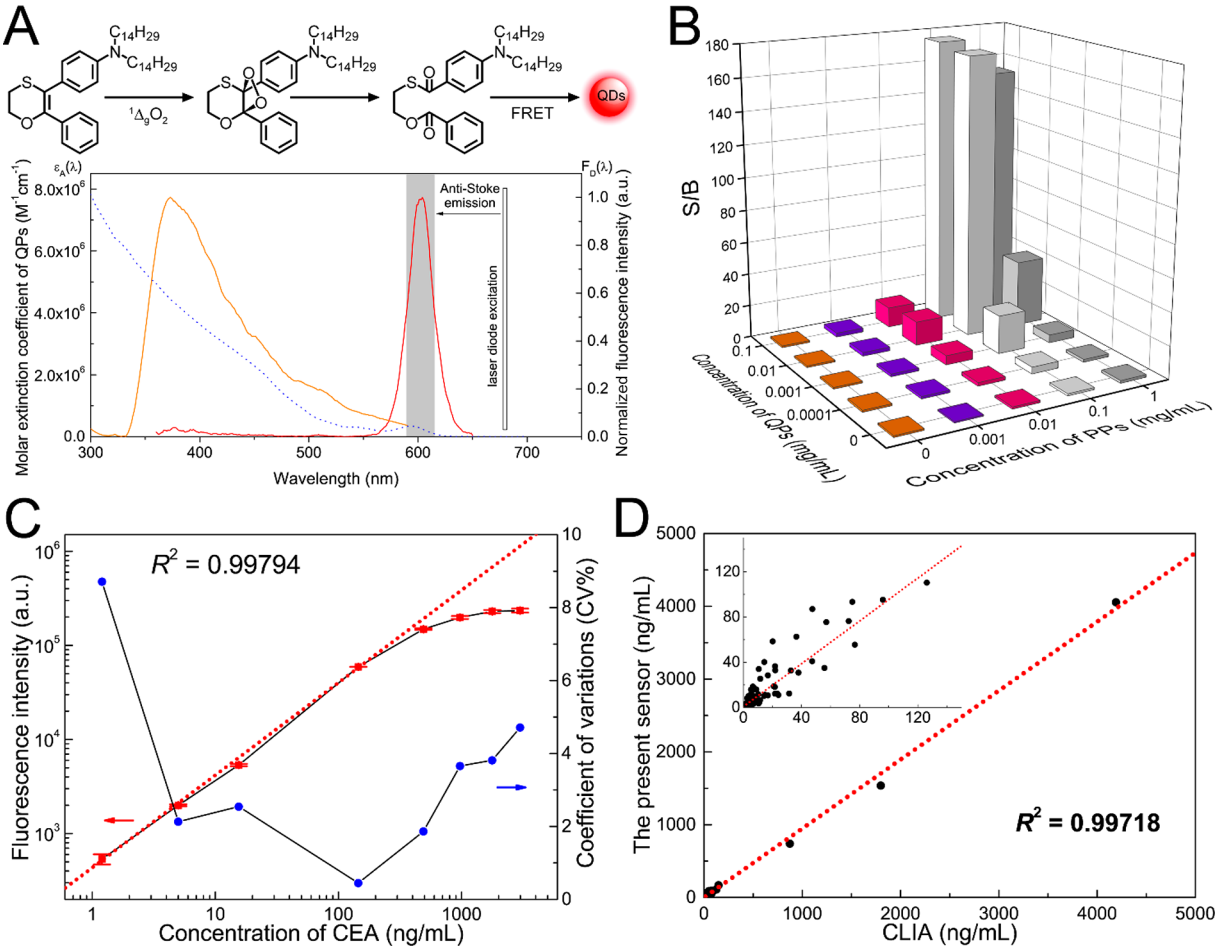

Figure 5. (A) FRET process within QPs (top panel) and emission spectrum of DTB, emission and excitation spectra of QDs (bottom panel). [The emission spectrum of DTB (orange solid curve) overlaps with the excitation spectrum of the QDs (blue dotted curve). The emission spectrum of the QDs (red solid curve) is separated from the DTB emission, and the sensitized emission of QDs can be measured using an optical band-pass filter (gray spectra in the background) within the QDs detection channel (605 ± 10 nm) and continuous laser excitation at 680 nm.] (B) Matrix titrations between PPs and QPs at fixed concentrations of CEA and biotinylated antibodies. (C) Standard curves for CEA and the intra-assay CV% for each concentration based on five replicates. (D) Comparison of CEA levels in 107 serum samples measured by the proposed method and those measured by CLIA.

attachment. Notably, CEA was chosen as the model analyst in biosensing and a biotin−streptavidin system was introduced to develop an assay format suitable for high-throughput screening, as well as to amplify the detection signal. The PPs and QPs were conjugated to streptavidin (SAv) and anti-CEA monoclonal antibodies (McAb), respectively. The coupling process was monitored by DLS analysis and is shown in Figure 4, parts A and B. The narrow width and symmetry of the scattering graph indicated that functional nanoparticles were highly monodisperse and no aggregation occurred during the conjugation process. Significant differences on measures of *Z*-average diameter and ζ-potential of QPs and PPs after protein coupling, indicating successful conjugation.

Flow cytometry analysis was conducted to examine the biological activity of the conjugated molecular after conjugation. QPs samples were incubated with fluorescein isothiocyanate (FITC)-labeled goat antimouse IgG, while the functional PPs samples were incubated with FITC-labeled goat antimouse IgG and biotinylated antibodies. As shown in Figure 4C, most of the QPs and PPs were conjugated with antibodies or streptavidin. The fluorescence intensity of each bead was recorded, and the mean fluorescence intensities (MFIs) of the functional nanoparticles were about 100−1000 times brighter than those of the negative beads, suggesting that nanoparticles-conjugated biomolecules retain a high biological activity after labeling.

FRET Process within QPs. DTB, the ditetradecyl derivative of thiophene (Figure 5A), was encapsulated into the particles along with the QDs. DTB reacts rapidly with singlet oxygen, as shown in Figure 5A. The chemiluminescence quantum yield of the ester derivative of DTB, formed during irradiation of DTB in 100 nM SiPc in chloroform, was determined relative to FITC and was calculated to be 0.067.

The broad excitation range of the QDs and the broad emission range of DTB lead to a long Förster distance, i.e., the distance at which the energy transfer efficiency is 50%. The Förster distance is expressed as the following equation:[37,38]

$$R_0^{\,6} = \frac{9\ln 10}{128\pi^5 N_A}\frac{\kappa^2 Q_D}{n^4}\mathcal{J}(\lambda) \quad (1)$$

where N_A is Avogadro's number, κ^2 is the dipole orientation factor, which is usually assumed to be 2/3, Q_D is the quantum yield of the donor in the absence of the acceptor, n is the

DOI: 10.1021/acs.analchem.9b00010
Anal. Chem. 2019, 91, 5777−5785

Table 1. Precision and Analytical Recovery of the Present Biosensor

	intra-assay precision			interassay precision				analytical recovery		
sample (ng/mL)	mean	SD	CV (%)	mean	SD	CV (%)	sample (ng/mL)	expected (ng/mL)	obsd (ng/mL)	recovery (%)
A (2.555)	2.764	0.064	2.315	2.247	0.125	5.563	D (20.93)	100.0	107.6	107.6
								300.0	313.5	104.5
								400.0	397.4	99.35
B (17.30)	17.22	0.237	1.376	16.35	0.594	3.633	E (47.28)	100.0	100.3	100.3
								300.0	290.3	96.77
								400.0	403.2	100.8
C (145.3)	146.8	6.571	4.476	136.2	2.901	2.130	F (72.47)	100.0	102.1	102.1
								300.0	324.6	108.2
								400.0	389.1	97.28

refractive index of the medium, and $\mathcal{J}(\lambda)$ is the spectral overlap integral from 350 to 640 nm, and is calculated as

$$\mathcal{J}(\lambda) = \frac{\int f_D(\lambda)\varepsilon_A(\lambda)\lambda^4 \, d\lambda}{\int f_D(\lambda) \, d\lambda} = \int \overline{f_D}(\lambda)\varepsilon_A(\lambda)\lambda^4 \, d\lambda \quad (2)$$

where f_D is the donor emission spectrum, $\overline{f_D}$ is the donor emission spectrum normalized to an area of 1, and ε_A is the acceptor molar extinction coefficient. According to the spectral overlap as shown in Figure 5A, where the wavelength is expressed in nanometers and ε_A in units of reciprocal moles per centimeter (M^{-1} cm^{-1}), we calculated that $\mathcal{J}(\lambda) = 7.55 \times 10^{16}$ M^{-1} cm^{-1} nm^4. Thus, R_0 = 67.50 Å, which is within the range of typical values (between 20 and 100 Å).

The efficiency (E_{FRET}) of DTB−QDs FRET can be expressed as

$$E_{FRET} = \frac{1}{1 + (R/R_0)^6} \quad (3)$$

where R is the distance between DTB and the QDs. From eq 3, R was calculated to range from 3.37 to 13.5 nm when E_{FRET} is in the range of 1.5−98.5%. Therefore, the use of QPs to encapsulate a large quantity of DTB and QDs is in theory predicted to sensitize the FRET process.

Homogeneous Biosensing. The feasibility of this biosensor was further verified using goat antimouse IgG biotinylated antibody under various conditions. The reaction mixtures are given in Table S1. The original fluorescence intensity and the signal-to-background ratio (S/B) of each group are shown in Figure S3. As shown in Figure S3, with biotinylated secondary antibody, the assay gave a much better signal as well as the S/B ratio under various conditions. Notably, measurable fluorescence signal was observed in the assays with naked PPs, even though the S/B ratios of groups E/e and F/f were approximately equivalent to 1. Two possible scenarios may be attributed to this. First, bare PPs, which were fabricated by encapsulating photosensitizer into latex nanospheres, would adsorb proteins and other biomolecules during the incubation, thereby enhancing the signal. In a second possible scenario, the intensity of the measured fluorescence signal depends on the relative distance between QPs and PPs in solution; thus, free QPs and PPs may shorten their relative distance at high concentration of beads, resulting in high background signal.

As illustrated in Figure 1, to quantify the biomarker in human serum, a homogeneous sandwich-type immunoassay has been constructed. The assay was performed in opaque 96-well microtiters. Samples were prepared by mixing functionalized QPs with biotinylated antibodies and were incubated with shaking. Antigen in the samples was captured by the antibodies and formed ternary complexes denoted "biotinylated McAb−CEA−functional QPs". Then, PPs-SAv were added in the absence of light, and the mixture was incubated in order to complete the streptavidin−biotin reaction. The assays were performed on a multimode plate reader (EnSpire/PerkinElmer). In the presence of target analyst, the $^1\Delta_gO_2$ molecules formed by irradiation at 680 nm and diffused only a short distance before being captured by the QPs, which provoke subsequent FRET within the QPs. The relative concentration of $^1\Delta_gO_2$ decreased rapidly with increasing distance from the surfaces of the PPs and could not be detected beyond about 200 nm from the PPs.[39] Thus, the free QPs did not contribute to the signal. In principle, the fluorescence signals were proportional to the concentrations of antigens in the samples. The FESEM micrographs and DLS data indicate the successful assembly of the biosensor (Figure S4).

Analytical Performance and Clinical Serum Samples Detection. Free PPs and QPs may shorten their relative distance and induce nonspecific detection signals at high concentrations of particles. To achieve an optimal S/B ratio, we conducted the matrix titrations between functional PPs and QPs at fixed concentrations of CEA (50 ng/mL) and biotinylated antibodies (125 ng/well). As shown in Figure 5B, the S/B ratio approached a plateau when the concentrations of functional PPs and QPs were 0.1 and 0.01 mg/mL, respectively. The hook effect was observed when the CEA concentration exceeded 490 ng/mL. Standard curves were determined based on the measurements of a series of standard which contained known concentrations of CEA (0, 1.2, 5, 15.5, 145, and 490 ng/mL). Standard curve constructions were carried out using linear regression on log−log transformations. For the best linear fitting curve under optimal conditions plotted in Figure 5C, the equation of calibration was described as $\log(Y) = 2.63762 + 0.95514 \log(X)$ ($R^2 = 0.99794$, $P < 0.0001$). Note that the error bars in Figure 5C denoted the standard deviation (SD, $n = 5$), and the coefficient of variation (CV) values are also displayed. The limits of detection (LODs), which were defined as mean value plus 3 times the SDs ($n = 30$) of the blank standard signal, were quantitated to be 0.046 ng/mL. These results indicated that this novel biosensor provided excellent analytical sensitivity and linearity in CEA detection. At each concentration level, the CVs were all less than 10%.

The precision of this biosensor was investigated based on intra-assay (repeatability) and interassay (reproducibility) validation. Three authentic samples were measured to

DOI: 10.1021/acs.analchem.9b00010
Anal. Chem. 2019, 91, 5777−5785

determinate the precision (three samples with five replicates were measured in a single run for intra-assay study, and the same samples with 10 replicates were measured in separate runs on five sequential days for interassay study). The CV values were recorded and are shown in Table 1. All the CVs were less than 10%. Furthermore, the analytical recovery was studied by adding purified CEA antigens to three measured serum samples. The recoveries of the spiking analyte were determined and are present in Table 1. The recoveries of the spiked analytes settled into the range of 90−110%. These results demonstrate that this biosensor is reliable.

To demonstrate the clinical application of this sensor, 107 serum samples were measured by the proposed method. The results were compared with those obtained using a commercially available CLIA kit. The correlations between the CEA values obtained by the two methods are presented in Figure 5D. The regression equation was $Y = 0.76307 + 0.94692X$ ($R^2 = 0.99718$, $P < 0.0001$, $n = 107$). These results demonstrate the excellent performance of the present biosensor for the measurement of CEA in human serum in a clinical setting.

Notably, this biosensor is initiated by a 680 nm diode laser and emit 605 nm anti-Stokes fluorescence as detecting signal, which is distinct from conventional FRET-based immunoassays or chemiluminescence resonance energy transfer (CRET).[40−42] The nanobiosensor reported here offers several unique advantages over CRET/FRET-based systems for biomolecular sensing. First of all, common FRET-based methods are not suitable for biomacromolecule detection because of their short Förster distance (<10 nm typically). To achieve the optimal S/B ratio, washing processes are recommended in FRET. However, as mentioned above, such procedures may result in poor specificity and sensitivity. For CRET, the detection relies on the distance and affinity between the enzymes and the substrate, and the Förster distance between the energy donor and acceptor is much shorter than that in FRET due to its poor energy-transfer efficiency and the limited number of energy acceptors. All of these factors severely limit the application of CRET. In contrast, for the biosensors reported here, two kinds of polystyrene nanoparticles, photosensitizer particles (PPs) and QD-doped particles (QPs), were prepared for sensing biomolecules in clinical sample matrixes. Great amounts of FRET donors and acceptors are both trapped in one nanosphere, which guarantees the efficacy and stability of FRET. Furthermore, the polystyrene beads in nanoscale suspended in the analytical solution provided an extremely large surface area, which enabled more biomolecules to be immobilized on the surface and provide more space for ligand docking and binding. Last but not least, the use of the 680 nm excitation wavelength minimized the interference from serum matrixes and led to an appreciable improvement of the sensitivity and precision in biosensing.

For specific and sensitive biomarker detection in homogeneous sandwich assays, antibodies remain the biomolecule of choice. The present biosensor could be adapted to detect any other biomarker by changing the specific antibodies, or be used for monitoring the interactions between biomolecules, including hybridization of nucleic acids. Furthermore, benefiting from size-dependent emission and broad excitation of colloidal QDs, this novel biosensor could be readily applied to multiplexed detection. Additionally, the biotin−streptavidin system of this sensor should permit straightforward automation using existing technology, including automatic dilution of samples and pipetting of reagents, which would further reduce the LOD and broaden the dynamic range. Moreover, the scale and morphology of the nanospheres could be further controlled and optimized by through changing encapsulation strategy and parameters. Once the size of the PPs and QPs are decreased to 100 nm or below, in vivo applications should be realized using this biosensor.

CONCLUSIONS

In this study, a highly sensitive and precise biosensor has been developed and a model homogeneous assay was constructed for quantitative determination of CEA in serum samples. This biosensor, based on nanotechnology, is advantageous not only for the relatively low cost, simplicity, and rapidity of its homogeneous format but also for the unique optical properties of QDs in biosensing. Similar to upconversion particles, the present biosensor emits light of shorter wavelength (605 nm) than the excitation (680 nm), promising the low background signal and the extraordinary sensitivity. In the case of CEA determination presented here, this nanobiosensor gave excellent linearity over the range of 1.2−490 ng/mL and displayed an LOD of 0.046 ng/mL, which is far more than adequate for meeting diagnostic requirements. The LOD of this sensor in CEA detection was even lower than that of fully optimized commercial immunoassay kits (e.g., Roche Elecsys CEA kit). The performance of the present biosensor also compared favorably with that of a commercial CLIA kit in analyzing 107 serum samples.

It should be noted that the assembly of QPs requires further optimization as well as the composition of the storage and detection reagents, seeing that the QPs showed the occasional tendency to aggregate. While the further improvement is undoubtedly required for the current biosensor, after it is completed, we expect the developed version of this nanotechnology-based, rapid, flexible, multiplex, and sensitive biosensor to be utilized for efficient early disease detection and high-throughput screening in medicine.

ASSOCIATED CONTENT

Supporting Information

The Supporting Information is available free of charge on the ACS Publications website at DOI: 10.1021/acs.analchem.9b00010.

Z-average size, polydispersity index, and ζ-potential of undoped CM-Ps and QPs, effect of encapsulating time, concentration of hexane, and the usage of QDs for the optimization of QPs, validation of the sensor, confirmation of the successful assembly of this nanospheres-based biosensor, reaction mixtures, and comparison between the current detection assay and other previously reported methods (PDF)

AUTHOR INFORMATION

Corresponding Authors

*Phone: 0086-20-62789355. Fax: 0086-20-37247604. E-mail: liutc@smu.edu.cn.

*Phone: 0086-20-62789355. Fax: 0086-20-37247604. E-mail: wg@smu.edu.cn.

ORCID

Tiancai Liu: 0000-0002-2985-3766

DOI: 10.1021/acs.analchem.9b00010
Anal. Chem. 2019, 91, 5777−5785

Author Contributions

[§]T.L. and Y.W. contributed equally to this work.

Notes

The authors declare no competing financial interest.

■ ACKNOWLEDGMENTS

This work was financially supported by the National Natural Science Foundation of China (Grant Nos. 81702072, 81271931, and 21575058).

■ REFERENCES

(1) Brus, L. E. *J. Chem. Phys.* **1984**, *80* (9), 4403−4409.
(2) Ben-Ari, E. T. *J. Natl. Cancer Inst.* **2003**, *95* (7), 502−504.
(3) Murray, C. B.; Kagan, C. R.; Bawendi, M. G. *Annu. Rev. Mater. Sci.* **2000**, *30* (1), 545−610.
(4) Hoshino, K.; Gopal, A.; Glaz, M. S.; Vanden Bout, D. A.; Zhang, X. *Appl. Phys. Lett.* **2012**, *101* (4), 043118.
(5) Marchuk, K.; Guo, Y.; Sun, W.; Vela, J.; Fang, N. *J. Am. Chem. Soc.* **2012**, *134* (14), 6108−6111.
(6) Michalet, X.; Pinaud, F. F.; Bentolila, L. A.; Tsay, J. M.; Doose, S.; Li, J. J.; Sundaresan, G.; Wu, A. M.; Gambhir, S. S.; Weiss, S. *Science (Washington, DC, U. S.)* **2005**, *307* (5709), 538−544.
(7) Walling, M.; Novak, J.; Shepard, J. *Int. J. Mol. Sci.* **2009**, *10* (2), 441−491.
(8) Medintz, I. L.; Uyeda, H. T.; Goldman, E. R.; Mattoussi, H. *Nat. Mater.* **2005**, *4* (6), 435−446.
(9) Jin, Z.; Hildebrandt, N. *Trends Biotechnol.* **2012**, *30* (7), 394−403.
(10) Hasegawa, M.; Tsukasaki, Y.; Ohyanagi, T.; Jin, T. *Chem. Commun.* **2013**, *49* (3), 228−230.
(11) Selvan, S. T.; Tan, T. T.; Ying, J. Y. *Adv. Mater.* **2005**, *17* (13), 1620−1625.
(12) Tortiglione, C.; Quarta, A.; Tino, A.; Manna, L.; Cingolani, R.; Pellegrino, T. *Bioconjugate Chem.* **2007**, *18* (3), 829−835.
(13) Shen, H.; Jawaid, A.; Snee, P. T. *ACS Nano* **2009**, *3* (4), 915−923 Supporting Information .
(14) Siegel, R. L.; Miller, K. D.; Jemal, A. *Ca-Cancer J. Clin.* **2018**, *68* (1), 7−30.
(15) Yoon, J. H.; Ham, I. H.; Kim, O.; Ashktorab, H.; Smoot, D. T.; Nam, S. W.; Lee, J. Y.; Hur, H.; Park, W. S. *Gastric Cancer* **2018**, *21*, 956−967.
(16) Jiang, X.; Yao, Z.; He, X.; Zhang, J.; Xie, K.; Chen, J.; Cao, M.; Zhang, J.; Yie, S. *Arch. Gynecol. Obstet.* **2019**, *299*, 229−237.
(17) Kuroki, M.; Yamaguchi, A.; Koga, Y.; Matsuoka, Y. *J. Immunol. Methods* **1983**, *60* (1−2), 221−233.
(18) Li, L.; Bading, J.; Yazaki, P. J.; Ahuja, A. H.; Crow, D.; Colcher, D.; Williams, L. E.; Wong, J. Y. C.; Raubitschek, A.; Shively, J. E. *Bioconjugate Chem.* **2008**, *19* (1), 89−96.
(19) Huang, X.; Li, J.; Wang, F.; Hao, M. *J. BUON* **2018**, *23* (4), 985−991.
(20) Hou, J. Y.; Liu, T. C.; Lin, G. F.; Li, Z. X.; Zou, L. P.; Li, M.; Wu, Y. S. *Anal. Chim. Acta* **2012**, *734* (13), 93−98.
(21) Matsumoto, K.; Yuan, J.; Wang, G.; Kimura, H. *Anal. Biochem.* **1999**, *276* (1), 81−87.
(22) Wu, J.; Fu, Z.; Yan, F.; Ju, H. *TrAC, Trends Anal. Chem.* **2007**, *26* (7), 679−688.
(23) Gao, Y. C.; Yuan, Z. B.; Yang, Y. D.; Lu, H. K. *Scand. J. Clin. Lab. Invest.* **2007**, *67* (7), 741−747.
(24) Tozzoli, R.; Basso, S. M.; D'Aurizio, F.; Metus, P.; Lumachi, F. *Clin. Biochem.* **2016**, *49* (16−17), 1227−1231.
(25) Falzarano, R.; Viggiani, V.; Michienzi, S.; Longo, F.; Tudini, S.; Frati, L.; Anastasi, E. *Tumor Biol.* **2013**, *34* (5), 3093−3100.
(26) Nishizono, I.; Iida, S.; Suzuki, N.; Kawada, H.; Murakami, H.; Ashihara, Y.; Okada, M. *Clin. Chem.* **1991**, *37* (9), 1639−1644.
(27) Algar, W. R.; Malanoski, A. P.; Susumu, K.; Stewart, M. H.; Hildebrandt, N.; Medintz, I. L. *Anal. Chem.* **2012**, *84* (22), 10136−10146.
(28) Li, Z.; Wang, Y.; Liu, Y.; Zeng, Y.; Huang, A.; Peng, N.; Liu, X.; Liu, J. *Analyst* **2013**, *138* (17), 4732−4736.
(29) Sousa, J. C. L.; Vivas, M. G.; Ferrari, J. L.; Mendonca, C. R.; Schiavon, M. A. *RSC Adv.* **2014**, *4* (68), 36024−36030.
(30) Li, Z.; Wang, Y.; Zhang, G.; Han, Y. *J. Cent. South Univ. Technol.* **2010**, *17* (6), 1148−1154.
(31) Liu, T.-C.; Huang, Z.-L.; Wang, H.-Q.; Wang, J.-H.; Li, X.-Q.; Zhao, Y.-D.; Luo, Q. *Anal. Chim. Acta* **2006**, *559* (1), 120−123.
(32) Peng, X.; Wickham, J.; Alivisatos, P. *J. Am. Chem. Soc.* **1998**, *120* (98), 5343−5344.
(33) Chen, Z.; Liang, R.; Guo, X.; Liang, J.; Deng, Q.; Li, M.; An, T.; Liu, T.; Wu, Y. *Biosens. Bioelectron.* **2017**, *91*, 60−65.
(34) Wang, H. Q.; Wang, J. H.; Li, Y. Q.; Li, X. Q.; Liu, T. C.; Huang, Z. L.; Zhao, Y. Di. *J. Colloid Interface Sci.* **2007**, *316* (2), 622−627.
(35) Han, M.; Gao, X.; Su, J. Z.; Nie, S. *Nat. Biotechnol.* **2001**, *19* (7), 631−635.
(36) Wang, H. Q.; Huang, Z. L.; Liu, T. C.; Wang, J. H.; Cao, Y. C.; Hua, X. F.; Li, X. Q.; Zhao, Y. Di. *J. Fluoresc.* **2007**, *17* (2), 133−138.
(37) Clegg, R. M. *Lab. Tech. Biochem. Mol. Biol.* **2009**, *33*, 1−57.
(38) Schulman, S. G. *Photophysical Processes in Molecules in Solution*; Elsevier Ltd., 1977.
(39) Ullman, E. F.; Kirakossian, H.; Singh, S.; Wu, Z. P.; Irvin, B. R.; Pease, J. S.; Switchenko, A. C.; Irvine, J. D.; Dafforn, A.; Skold, C. N. *Proc. Natl. Acad. Sci. U. S. A.* **1994**, *91* (12), 5426−5430.
(40) Lee, J. S.; Joung, H. A.; Kim, M. G.; Park, C. B. *ACS Nano* **2012**, *6* (4), 2978−2983.
(41) Wegner, K. D.; Jin, Z.; Linden, S.; Jennings, T. L.; Hildebrandt, N. *ACS Nano* **2013**, *7* (8), 7411−7419.
(42) Wegner, K. D.; Lanh, P. T.; Jennings, T.; Oh, E.; Jain, V.; Fairclough, S. M.; Smith, J. M.; Giovanelli, E.; Lequeux, N.; Pons, T.; Hildebrandt, N. *ACS Appl. Mater. Interfaces* **2013**, *5* (8), 2881−2892.

DOI: 10.1021/acs.analchem.9b00010
Anal. Chem. 2019, 91, 5777−5785